Research Article | Vol. 27, No. 5 | 4 Mar 2019 | OPTICS EXPRESS 7642
Optics EXPRESS

Deriving inherent optical properties from classical water color measurements: Forel-Ule index and Secchi disk depth

SHENGLEI WANG,[1,2] ZHONGPING LEE,[3,*] SHAOLING SHANG,[4] JUNSHENG LI,[1] BING ZHANG,[1] AND GONG LIN[4]

[1]*Key Laboratory of Digital Earth, Institute of Remote Sensing and Digital Earth, Chinese Academy of Sciences, Beijing 100094, China*
[2]*Biological and Environmental Sciences, School of Natural Sciences, University of Stirling, Stirling, UK*
[3]*School for the Environment, University of Massachusetts Boston, Boston, MA 02125, USA*
[4]*State Key Laboratory of Marine Environmental Science, Xiamen University, Xiamen 361005, China*
**Zhongping.Lee@umb.edu*

Abstract: Secchi disk depth (Z_{SD}) and Forel-Ule index (*FUI*) are the two oldest and easiest measurements of water optical properties based on visual determination. With an overarching objective to obtain water inherent optical properties (IOPs) using these historical measurements, this study presents a model for associating remote-sensing reflectance (R_{rs}) with *FUI* and Z_{SD}. Based upon this, a scheme (FZ2ab) for converting *FUI* and Z_{SD} to absorption (a) and backscattering coefficients (b_b) is developed and evaluated. For a data set from HydroLight simulations, the difference is <11% between FZ2ab-derived a and known a, and <28% between FZ2ab-derived b_b and known b_b. Further, for a data set from field measurements, the difference is < 30% between FZ2ab-derived a and measured a. These results indicate that FZ2ab can bridge the gap between historical measurements and the focus of IOP measurements in modern marine optics, and potentially extend our knowledge on the bio-optical properties of global seas to the past century through the historical measurements of *FUI* and Z_{SD}.

1. Introduction

Obtaining long-term geophysical properties of water for the ocean is of great importance in studying the trend of marine primary production and carbon stocks and understanding the role of oceans in climate change [1,2]. For the global ocean, satellite measurement via ocean color is the only feasible means for synoptic and repetitive coverage, which is a key requirement for studying the temporal and spatial information on the bio-optical properties of the oceans [2–4]. Ocean color is fundamentally determined by inherent optical properties (IOPs), and variations of IOPs are indicators of changes in the optically active constituents of water. In particular, the absorption coefficient (a, m^{-1}) and backscattering coefficient (b_b, m^{-1}) play a key role in governing light propagation in water columns and they primarily determine remote-sensing reflectance (R_{rs}, sr^{-1}), a radiometric measure of water/ocean color [5,6]. Therefore, the derivation and understanding of IOPs have been the focus of ocean color remote sensing in the past decades [7–10]. Extensive efforts have been made in the recent decades to develop modern optical-electronic instruments for measuring IOPs [11–13] and robust algorithms for retrieving IOPs from remote-sensing reflectance (R_{rs}) (e.g., IOCCG, 2006). However, long before these developments in modern marine optics, earlier oceanographers used rudimentary techniques to obtain valuable measurements of the optical properties of water, represented by the Secchi disk and Forel-Ule color scale, and there are records of such measurements of world's oceans for more than a century [14–16].

The Secchi disk depth (Z_{SD}, m), a measure of water clarity, is "measured" by lowering a white or black-and-white disk with a diameter around 30 cm in water until it is no longer visible

#347078 https://doi.org/10.1364/OE.27.007642
Journal © 2019 Received 28 Sep 2018; revised 12 Dec 2018; accepted 13 Dec 2018; published 1 Mar 2019

Optics EXPRESS

to an observer at the surface. Z_{SD} provides an intuitive and quantitative measurement of water transparency or clarity, and its measurement started ~150 years ago [16]. Z_{SD} has been widely accepted and measured globally owing to its low cost and easy acquisition, maintaining a tradition of ongoing measurement and expanding applications through many science projects [17,18]. The theoretical interpretation of Z_{SD} was initiated about 60 years ago [19] and summarized in Preisendorfer [20], where Z_{SD} was theoretically modeled as an inverse function of the sum of beam attenuation (c, m^{-1}) and diffuse attenuation coefficient of downwelling irradiance (K_d, m^{-1}) weighted by the human eye response function. However, numerous measurements found that Z_{SD} is highly dependent on K_d rather than c [21–23]. This mismatch or inconsistency between theory and measurements was resolved recently [24,25], where mistakes in the classical Secchi theory and model were identified. The new Secchi theory and mechanistic model [24] indicate that Z_{SD} is determined by K_d at the transparent window (K_d^{tr}), which is in excellent agreement with the extensive measurements by various groups over a wide range of waters [25]. The transparent window indicates the spectral wavelength of a water body that is mostly penetrative by visible light, which can be determined from the spectrum of remote-sensing reflectance [24] and also can be expressed and calculated as the dominant wavelength of remote-sensing reflectance [26].

Around the end of the nineteenth century, the Forel-Ule scale was invented to systematically document color variations of natural waters. The Forel-Ule index (*FUI*) divides natural water color into 21 classes, covering water colors from dark blue to yellowish brown [27]. *FUI* is determined by comparing the appearance of water against a handheld Forel-Ule color scale while a Secchi disk is kept at half of Z_{SD}; the matching index in the color scale is recorded as the *FUI* of the water body under observation [16]. Because color is a perception of the human eye to the spectral radiance of any object, the *FUI* color index of water column itself without the Secchi disk now can be calculated based on water reflectance and the response function of the human eye [27,28]. It is noteworthy that *FUI* color index measurements have historically used a Secchi disk in order to enhance brightness, but a side effect of this protocol is that the color is slightly altered. However, studies have shown that the historical *FUI* can be simply linked with the *FUI* of water (i.e., without a Secchi disk in water for the determination of *FUI*) [29].

Because the color of water is an outcome of the interactions between sunlight and the absorption and scattering of water constituents, it varies with changes in the optically active constituents of water [26]. Given its long history, transferability in sensors, and high capacity for indicating natural events and bulk changes in water constituents at large-scales [15,30–32], *FUI* was recently included in a "standard" suite of water quality parameters. Further, owing to its ease of measurement, *FUI* is also included in the collections of water quality data from sensors developed for citizen science based observatories that include smartphone-based approaches [33].

Although both Z_{SD} and *FUI* are valuable measurements of some aspects of water properties, there is a gap between the historical data set and the focus of IOP measurements in modern marine optics. In general, *FUI* is a qualitative representation, which makes it difficult to compare *FUI* with quantitative measurements of IOPs developed in recent decades. This is also highlighted in Woerd and Wernand [34] (their Fig. 8) that there are large uncertainties between the absorption coefficient at 440 nm and the hue angle (a measure of water color). It is thus useful and necessary to convert the Z_{SD} and *FUI* data records to IOPs (a and b_b) to fill this gap, which can then potentially extend IOPs of the global oceans from present day to decades and a century ago. As R_{rs} is an analytical function of a and b_b, we thus developed an empirical model to express R_{rs} as a function of *FUI* and Z_{SD}. In addition, as Z_{SD} is an analytical function of K_d that can be expressed with a and b_b, this *FUI* to R_{rs} model offers a means of algebraically deriving $a\&b_b$ from the combination of $FUI\&Z_{SD}$. This paper thus presents the scheme to semi-analytically derive $a\&b_b$ from $FUI\&Z_{SD}$, termed as FZ2ab hereafter, which demonstrates the potential of obtaining IOPs from historical measurements.

Optics EXPRESS

2. Data sets

In this study, the FZ2ab scheme for retrieving $a\&b_b$ from $FUI\&Z_{SD}$ was developed and tested using three data sets.

The first data set (Dataset 1) is a field measured data set containing Z_{SD} and R_{rs} spectra from 612 sites covering clear to turbid waters from coastal and oceanic areas around the world. The waters of these measurements cover the China Sea, Gulf of Mexico, and the Pacific and Atlantic oceans (see Fig. 1 of [35]) with Chla (concentration of chlorophyll) in a range of ~0.02 μg/L to > 100 μg/L. The measurement and determination of R_{rs} followed the above-surface approach [36,37]. Z_{SD} values ranged from 0.3 m to 44.3 m with an average value of 10.6 m. Dataset 1 was used to develop the model for retrieving R_{rs} from FUI and Z_{SD}.

The second data set (Dataset 2) is a simulated data set including 500 data points generated by HydroLight [38] and published by the International Ocean Colour Coordinating Group (IOCCG) for the purpose of algorithm validation [39]. This simulated data set comprises both IOPs and apparent optical properties (AOPs). In particular, IOPs, including $a(\lambda)$ and $b_b(\lambda)$, were generated with established bio-optical models, whereas AOPs, including $K_d(\lambda)$ and $R_{rs}(\lambda)$, were generated using HydroLight with the available IOPs. IOP data covered a wide range of properties, with $a(440)$ ranging from ~0.01 to 3.2 m^{-1} and $b_b(440)$ ranging from 0.003 to 0.13 m^{-1}, which suggest an equivalent range of Chla concentration from ~0.03 to 30.0 μg/L. Z_{SD} of this data set was derived following Lee et al. [24] (ranging from ~0.8 m to 34.8 m with an average of 9.1 m).

The third one (Dataset 3) is a field measured data set covering 195 sites in oceanic and coastal waters off China (Fig. 1). It contains concurrent measurements of R_{rs}, Z_{SD}, and absorption coefficients (a). Details of the measurements are available in Shang et al. [40]. In brief, $a(\lambda)$ was obtained as the sum of the absorption coefficients of water (a_w), particulates (a_p), and colored dissolved organic matter (a_g). Specifically, a_p was measured with a dual-beam PE Lambda 950 spectrophotometer equipped with an integrating sphere (150 mm diameter) following a modified Transmittance–Reflectance (T-R) method [41,42], and a_g was measured using a Varian Cary-100 dual-beam spectrophotometer following Ocean Optics Protocols Version 2.0 [43]. This data set covered a Z_{SD} range from 0.1 to 30 m with an average of 9.9 m, whereas $a(440)$ from water samples ranged from ~0.01 to 3.9 m^{-1}. In particular, Dataset 3 from field measurements was independent from Dataset 1 used in the development of the model for R_{rs}. Dataset 2 and Dataset 3 were used to test the performance of the FZ2ab scheme. See Data File 1 and Data File 2 for underlying values in Dataset 1 and Dataset 3 respectively, in the Supplementary Material.

Optics EXPRESS

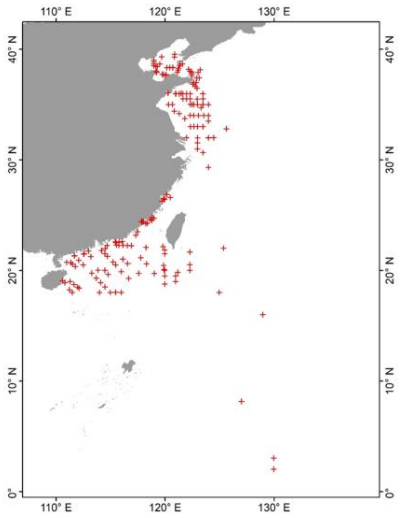

Fig. 1. Locations of 195 sampling sites from Dataset 3.

In the three data sets, the *FUI* was derived from the R_{rs} spectrum with the color response function of CIE [44] using the method described in Wang et al. [26]. In brief, an R_{rs} spectrum was converted to XYZ in CIE colorimetric space with the integration of the product of an R_{rs} spectrum and the color response function [44]. By normalizing the brightness of the spectrum, the chromaticity coordinate (x,y) was derived from X,Y,Z. Then, a color angle α was calculated from (x,y), and its corresponding *FUI* was derived using an updated 21-class *FUI* lookup table established from the color of the Forel-Ule scale by Novoa et al. [45]. Note that the *FUI* in this study represents an index of water color without the Secchi disk in water [26].

Meanwhile, R_{rs} at the transparent window (R_{rs}^{tr}) was determined as the R_{rs} value at the dominant wavelength, which is a wavelength indicating the perceived water color produced by the R_{rs} spectrum. The dominant wavelength is also well related to the color angle α and can be calculated from α using a reference table [26].

3. Model of R_{rs} based on *FUI* and Z_{SD}

According to the new theory of Secchi depth [24,25], Z_{SD} is an inverse function of K_d at the transparent window (K_d^{tr}). Further, K_d is a function of $a\&b_b$ based on radiative transfer [46–48]. Thus, another independent function of $a\&b_b$ is required at the transparent window in order to algebraically derive these two properties. *FUI* is a measure of water color, which in principle is analogous to R_{rs} – also a measure of water color. Studies have shown that *FUI* can be accurately calculated from an R_{rs} spectrum [27,28]. However, there is no model, theoretical or empirical, to convert *FUI* to R_{rs}, particularly at the transparent window of a water body (R_{rs}^{tr}). Here an empirical model based on a wide range of measurements is developed for this conversion through correlation analyses.

For the R_{rs}^{tr}, *FUI*, and Z_{SD} values of Dataset 1, various empirical relationships between R_{rs}^{tr} and *FUI* as well as between R_{rs}^{tr} and $FUI\&Z_{SD}$ were tested. It was found that the transparent window location of the water samples varied in a wide range, and the relationship between R_{rs}^{tr} and *FUI* was very scattered, the same with that between $R_{rs}^{tr}$and Z_{SD} (Fig. 2). But a strong correlation was found between R_{rs}^{tr} and $ln(FUI*Z_{SD})$ (see Fig. 3(a)), at least for the data set in this study. Hence, an empirical model for estimating R_{rs}^{tr} from *FUI* and Z_{SD} could be developed as follows:

Optics EXPRESS

$$R_{rs}^{tr} = 0.0045C^2 - 0.0383C + 0.0852$$
$$C = \ln(FUI \times Z_{SD}) \quad (1)$$

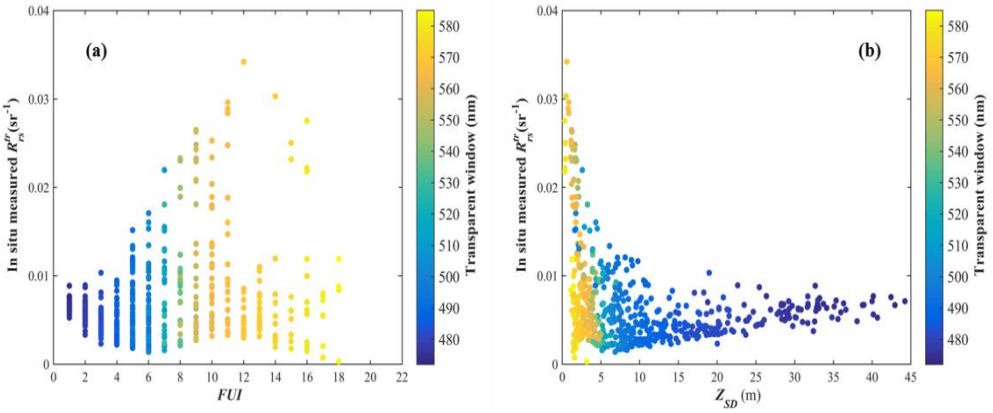

Fig. 2. Scatterplots of (a) in situ measured R_{rs}^{tr} versus *FUI*, (b) in situ measured R_{rs}^{tr} versus Z_{SD} based on the in situ data set (Dataset 1, N = 612).

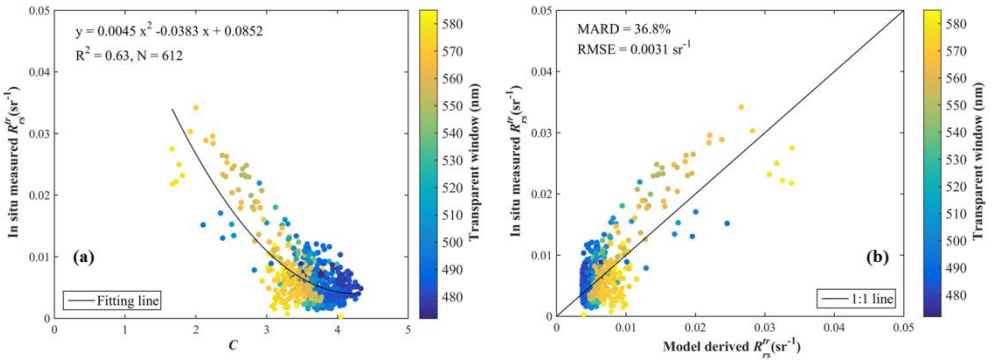

Fig. 3. Scatterplots of (a) in situ measured R_{rs}^{tr} versus *C* (i.e. $ln(FUI*Z_{SD})$), (b) in situ measured R_{rs}^{tr} versus the modelled R_{rs}^{tr} from the combination of *FUI* and Z_{SD} based on the in situ data set (Dataset 1, N = 612).

For this data set with wide dynamic ranges of Z_{SD} and *FUI*, the coefficient of determination (R^2) between known and modeled R_{rs}^{tr} was 0.63, with root mean square error (RMSE) of 0.0031 sr^{-1} and mean absolute relative difference (MARD) of 36.8%, as shown in Fig. 3(b). The accuracy indices RMSE and MARD are defined as follows:

$$RMSE = \sqrt{\frac{\sum_{i=1}^{n}\left(x_{est,i} - x_{mea,i}\right)^2}{n}} \quad (2)$$

$$MARD = \frac{1}{n}\sum_{i=1}^{n}\frac{2\left|x_{est,i} - x_{mea,i}\right|}{\left(x_{est,i} + x_{mea,i}\right)} * 100\% \quad (3)$$

where x_{est} denotes the estimated value, x_{mea} denotes the measured or simulated value, and n is the number of measurements.

These R^2 and RMSE values are very encouraging because *FUI* is primarily a qualitative measure of water color, where some small spectral variations in R_{rs} spectrum may not be well

Optics EXPRESS

represented in *FUI*. Further, the uncertainty of R_{rs} from satellite measurements, especially those of coastal waters, is also ~20–30% [49–52]. Therefore, these quality measures suggest the converted R_{rs}^{tr} from *FUI*&Z_{SD} are acceptable for further inversion practices.

4. Derivation of *a* and b_b from Z_{SD} and *FUI*

Based on the new Secchi disk depth model [24,25], Z_{SD} can be approximated as:

$$Z_{SD} = \frac{0.96}{K_d^{tr}} \tag{4}$$

As mentioned before, K_d^{tr} is the diffuse attenuation coefficient of downwelling irradiance at the transparent window of the water body, which has been recognized as the governing parameter of Z_{SD} in the new theory and model [24,25], as it suggests that Z_{SD} is determined by photons in the transparent window rather than photons of the entire visible domain.

Further, modeling of the radiative transfer equation suggested K_d can be expressed as a function of a and b_b [47,48]:

$$\boldsymbol{K_d}(\boldsymbol{\lambda}) = (1+\mathbf{m}_0 \times \boldsymbol{\theta_s})\boldsymbol{a}(\boldsymbol{\lambda}) + \boldsymbol{m}_1 \times \left(1-\boldsymbol{\gamma}\frac{\boldsymbol{b_{bw}}(\boldsymbol{\lambda})}{\boldsymbol{b_b}(\boldsymbol{\lambda})}\right)\left(1-\boldsymbol{m}_2 \times e^{-\boldsymbol{m}_3 \times \boldsymbol{a}(\boldsymbol{\lambda})}\right) * \boldsymbol{b_b}(\boldsymbol{\lambda}) \tag{5}$$

where $m_{0\text{-}3}$ are model constants, and $\boldsymbol{\theta_s}$ is the solar zenith angle.

Decades of ocean optics studies have shown that R_{rs} is related to a and b_b through below-surface remote-sensing reflectance (r_{rs}) [5,8]:

$$\boldsymbol{R_{rs}}(\boldsymbol{\lambda}) = \frac{0.52\,\boldsymbol{r_{rs}}(\boldsymbol{\lambda})}{1-1.7\boldsymbol{r_{rs}}(\boldsymbol{\lambda})} \tag{6a}$$

$$\boldsymbol{r_{rs}}(\boldsymbol{\lambda}) = (\boldsymbol{g}_0 + \boldsymbol{g}_1 \frac{\boldsymbol{b_b}(\boldsymbol{\lambda})}{\boldsymbol{a}(\boldsymbol{\lambda})+\boldsymbol{b_b}(\boldsymbol{\lambda})})\frac{\boldsymbol{b_b}(\boldsymbol{\lambda})}{\boldsymbol{a}(\boldsymbol{\lambda})+\boldsymbol{b_b}(\boldsymbol{\lambda})} \tag{6b}$$

Here, g_0 and g_1 are approximately 0.089 and 0.125, respectively.

Thus, with R_{rs}^{tr} derived from known *FUI* and Z_{SD} using Eq. (1) and K_d^{tr} calculated from Z_{SD} (Eq. (4)), we have two equations (Eq. (5) and Eq. (6)) for two unknowns (a^{tr}, b_b^{tr}), which can then be derived algebraically from known pairs of Z_{SD} and *FUI*.

5. Evaluation of the FZ2ab inversion scheme

5.1 Evaluation with HydroLight data set

The FZ2ab inversion scheme was first evaluated using Dataset 2. Because R_{rs}^{tr} is a required input in the derivation of a&b_b in FZ2ab and converted from *FUI*&Z_{SD}, we first compared model (Eq. (1)) derived R_{rs}^{tr} with known (HydroLight simulated) R_{rs}^{tr}; Fig. 4 shows a scatterplot between the two. The MARD and RMSE for the estimated R_{rs}^{tr} were 40.3% and 0.0042 sr^{-1}, respectively, which are similar to those observed during the development of the model. Considering that the simulated data set includes quite random combinations of optically active constituents (i.e., colored dissolved organic matter, phytoplankton, suspended sediments) that may not exist in natural environments, these statistical measures suggest acceptable model results for R_{rs}^{tr}. On the other hand, for an R_{rs} spectrum, *FUI* itself is more dependent on the spectral shape rather the entire magnitude. Therefore, the modeled R_{rs}^{tr} from *FUI* is expected to have some uncertainties.

Optics EXPRESS

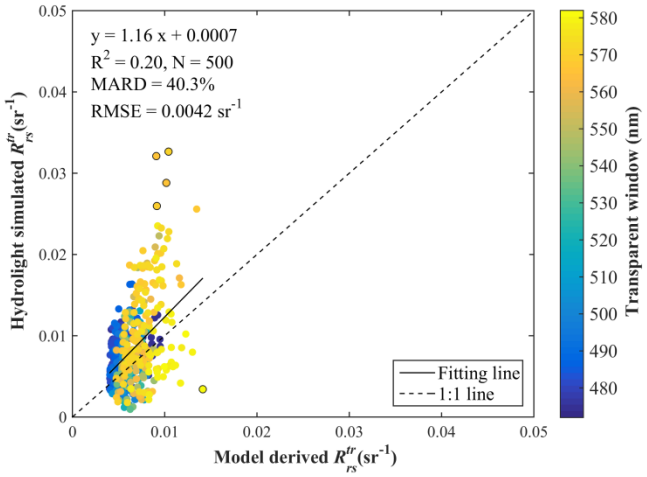

Fig. 4. Scatterplot between R_{rs}^{tr} from HydroLight simulation and R_{rs}^{tr} obtained from FZ2ab scheme. The five black outlined circles were considered as outliers with extreme combinations of optically active constituents (i.e., colored dissolved organic matter, phytoplankton, and suspended sediments). If excluded, MARD would decrease from 40.3% to 39.6%.

A comparison of FZ2ab derived a^{tr} and known a^{tr} (in a range of ~0.02–0.83 m^{-1}) for the HydroLight simulated data set is shown in Fig. 5, where the MARD value is 10.5%, RMSE is 0.034 m^{-1}, and R^2 is 0.95. For such a wide range of a^{tr}, these values indicate excellent retrieval of a^{tr} by FZ2ab, even though the input estimated R_{rs}^{tr} has relatively large errors. Note that the a^{tr} derived by FZ2ab is slightly (~9.9%) lower than known a^{tr} at the high end (a^{tr} > ~0.4 m^{-1}). This is because the *FUI* values for these data points ranged 18–21, which are beyond the *FUI* range used in the development of the model (Eq. (1)) to calculate R_{rs}^{tr} from *FUI* and Z_{SD}. Meanwhile, there was a small (12.4%) overestimation at the lower end when a^{tr} < ~0.08 m^{-1}, which corresponds to R_{rs}^{tr} < 0.01 sr^{-1}, where the model estimated R_{rs}^{tr} was underestimated compared to HydroLight simulations (see both Fig. 3 and Fig. 4). These biases could be improved in the future by refining Eq. (1) with more inclusive data.

Unlike the excellent retrieval of a^{tr}, the performance of FZ2ab in the retrieval of b_b^{tr} (0.002–0.133 m^{-1}) was less robust (Fig. 6). MARD was 28.0%, R^2 was 0.78, and RMSE was 0.014 m^{-1}, but most data points fall around the 1:1 line. This difference between the performance of FZ2ab for a^{tr} and b_b^{tr} retrieval is a result of the combined effects of the following: 1) $K_d(\lambda)$ is determined by both $a\&b_b$, but $a(\lambda)$ plays a dominant role, and thus Z_{SD} (i.e., K_d^{tr}) provides a first order estimation of a^{tr}, where the application of R_{rs}^{tr} (i.e., *FUI*) helps in correcting the contribution of b_b^{tr} in K_d^{tr}; 2) in general, $R_{rs}(\lambda)$ depends on the ratio of $b_b(\lambda)/a(\lambda)$, and thus, the value of R_{rs}^{tr} can be impacted by both a^{tr} and b_b^{tr}. Therefore, the uncertainty brought by the R_{rs}^{tr} estimation has a smaller impact on the retrieval of a^{tr} (which is mainly determined by K_d^{tr}), but a larger impact on the retrieval of b_b^{tr} as it is proportional to R_{rs}^{tr}.

Optics EXPRESS

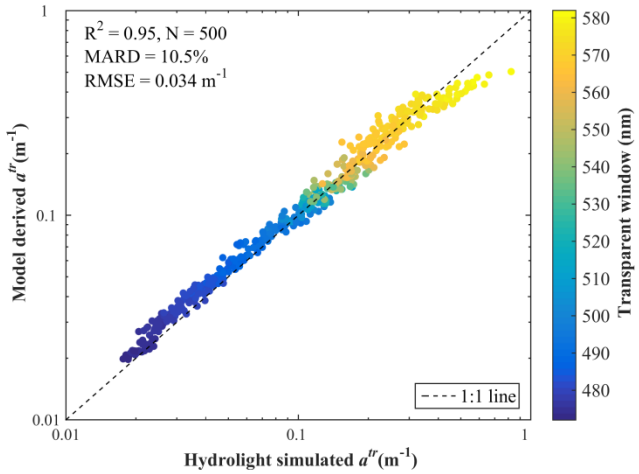

Fig. 5. Scatterplot of FZ2ab derived a^{tr} versus HydroLight a^{tr} for the simulated data set.

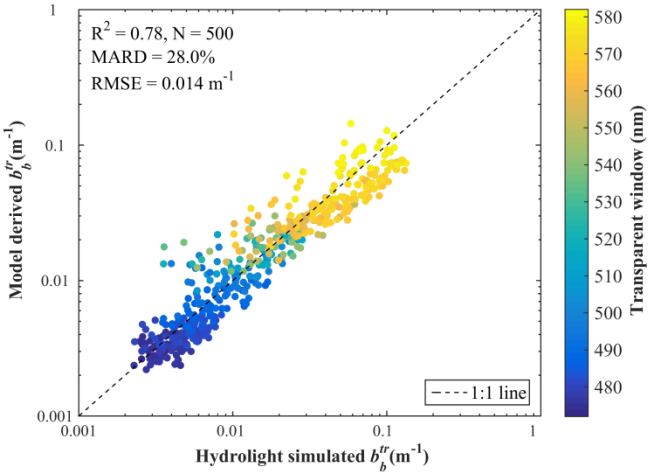

Fig. 6. Scatterplot of FZ2ab derived b_b^{tr} versus HydroLight b_b^{tr} for the simulated data set.

5.2 Evaluation with the field data set

The FZ2ab system was further tested and evaluated with Dataset 3. Figure 7 compares modeled vs measured R_{rs}^{tr}, and Fig. 8 compares modeled vs measured a^{tr}. The modeled R_{rs}^{tr} was found to match measured R_{rs}^{tr} quite well for this field data set, with MARD value of 27.3%, RMSE of 0.0036 sr^{-1}, and R^2 as 0.83. The higher performance of the measured data set is likely because field data were collected in natural environments, where extreme combinations of phytoplankton and suspended sediments that occurred in the simulation could be avoided. Nevertheless, when R_{rs}^{tr} < ~0.005 sr^{-1}, the model derived R_{rs}^{tr} was found to be overestimated (by ~48.9%) compared with the known R_{rs}^{tr}, as presented in the scatter plot for R_{rs}^{tr} at the lower end. Similarly with the results of the HydroLight data set, the uncertainties in R_{rs}^{tr} estimation did not significantly affect the estimated a^{tr} (0.01–0.76 m^{-1}), for which a robust performance (R^2 = 0.88, MARD = 26.0%) has been achieved. Taking into account uncertainties in the measurements of R_{rs} [53,54] and a from water samples [55], these results suggest that the a^{tr} and R_{rs}^{tr} values estimated from the FZ2ab system are basically consistent with those from

Optics EXPRESS

sample measurements. Unfortunately, we could not acquire field measured b_b to test and validate the b_b^{tr} retrievals.

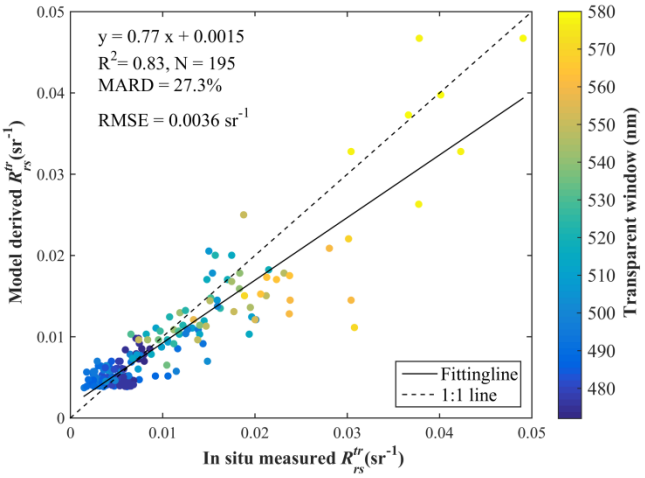

Fig. 7. Scatterplot of modeled R_{rs}^{tr} versus measured R_{rs}^{tr} based on Dataset 3.

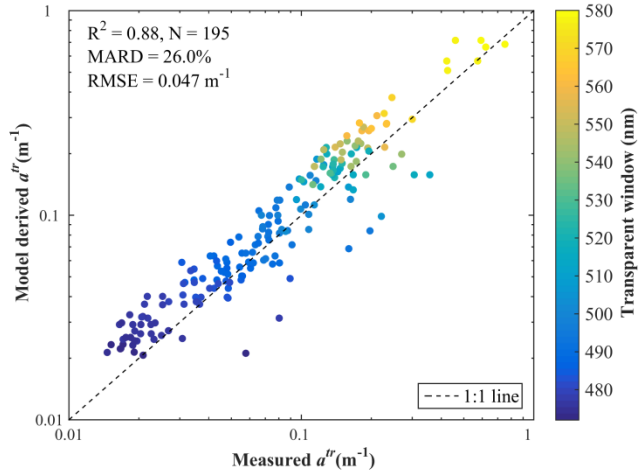

Fig. 8. Scatterplot of FZ2ab derived a^{tr} versus measured a^{tr} from water samples in Dataset 3.

6. Discussion and conclusions

Global oceanographic measurements play a key role in the research of climate change, where consistent and meaningful data covering long time spans are critical [56,26]. Taking full advantage of historical data collected over the past century, especially before the era of satellite-based measurements, is quite necessary to extend the period of effective records [56,57]. Water color and transparency are the few oceanographic parameters closely coupled with the physical and biogeochemical processes at different spatial and temporal scales that have been recorded for more than a century [58]. Therefore, the effective use of such historical measurements would provide important insights into the status and trend of oceanic environments over a long time scale.

In the past decades, realizing the intuitive and quantitative representation of Z_{SD}, a series of studies used the long record of Z_{SD} to study phytoplankton in the oceans [27,57]. However,

Optics EXPRESS

because of multiple factors affecting the value of Z_{SD}, the empirically converted Chla from Z_{SD} exhibited different levels of uncertainties for different regions. On the other hand, probably due to the subjective and qualitative nature of *FUI*, only few studies used the long record of *FUI* to study the status or trend of water quality or phytoplankton in marine environments. Further, studies have shown the potential of *FUI* and Z_{SD} to indicate changes in bulk water optical properties, especially at large scales [27,28,59]. Here, for the first time, a scheme (FZ2ab) was developed to semi-analytically derive the total absorption coefficient (a) and back scattering coefficient (b_b) from the combination of *FUI* and Z_{SD}. Such a scheme will not only offer a route to extend IOPs of the oceans back to a century ago, but the derived absorption coefficient could also improve the estimation of Chla, which has been widely and routinely used to represent biomass in aquatic environments.

As would be expected, although both *FUI* and Z_{SD} are closely related to an R_{rs} spectrum, R_{rs}^{tr} values derived from *FUI*&Z_{SD} have some uncertainties. This is because some spectral variations of the R_{rs} spectrum cannot be fully reconstructed from a 21-class *FUI* system, especially when this system was used to estimate the R_{rs} value at an everchanging wavelength. The uncertainty appears to be the highest for the data set in this study when the R_{rs}^{tr} value is under 0.01 sr^{-1} (see Figs. 3, 4, 7) where the value of $ln(FUI*Z_{SD})$ is between 3 and 4. This is likely a result that when $ln(FUI*Z_{SD})$ is 3 to 4, the dominant wavelength of the transparent window changes over a wide range (470 nm ~580 nm), indicating the complicated and varying constituents in water. Moreover, observation conditions, such as the sky condition and the viewing geometry that may affect either *FUI* and/or R_{rs}^{tr}, were not taken into consideration in the reconstruction of R_{rs}^{tr} [60]. Nevertheless, the estimated R_{rs}^{tr} showed MARD values of just 27.3% and 40.3% for the field measured data set and HydroLight simulated data set, respectively. However, the analytical optical mechanism behind this R_{rs}^{tr} derivation model remains to be studied in the future work, which may refine this model and improve the R_{rs}^{tr} estimation accuracy.

More importantly, it is very encouraging that the uncertainties in model derived R_{rs}^{tr} do not significantly affect the subsequent derivation of a^{tr} in the FZ2ab scheme. This is because Z_{SD} is mainly determined by a^{tr}. For instance, an increase of 50% in R_{rs}^{tr} only decreases the retrieved a^{tr} by ~13.6% with this FZ2ab scheme. Therefore, small MARD values were observed for the FZ2ab-estimated a^{tr}, i.e. 10.5% and 24.8% for the simulated data set and field measured data set, respectively. However, because b_b^{tr} is proportional to R_{rs}^{tr}, where an increase in R_{rs}^{tr} by 50% will increase the retrieved b_b^{tr} by ~28.2% with the FZ2ab scheme. As a result, the MARD of estimated b_b^{tr} was larger (28.0%) than that of simulated a^{tr}. Moreover, it is found that the retrieval performance (for the entire a^{tr} and b_b^{tr} range in this study) is not sensitive to *FUI*, where MARD value for the first 1-9 *FUI* is nearly the same as that of all *FUI*. This result suggests nearly uniform performance for both oceanic waters and coastal waters. Overall, the results indicate that in the FZ2ab system, through simultaneously resolving the equations of R_{rs}^{tr} and Z_{SD} (Eq. (5) and Eq. (6)), the impact of R_{rs}^{tr} uncertainty can be reduced when a^{tr} and b_b^{tr} are derived. This also implies that Z_{SD} plays a larger role than *FUI* in determining the values of a^{tr} and b_b^{tr}.

Optics EXPRESS

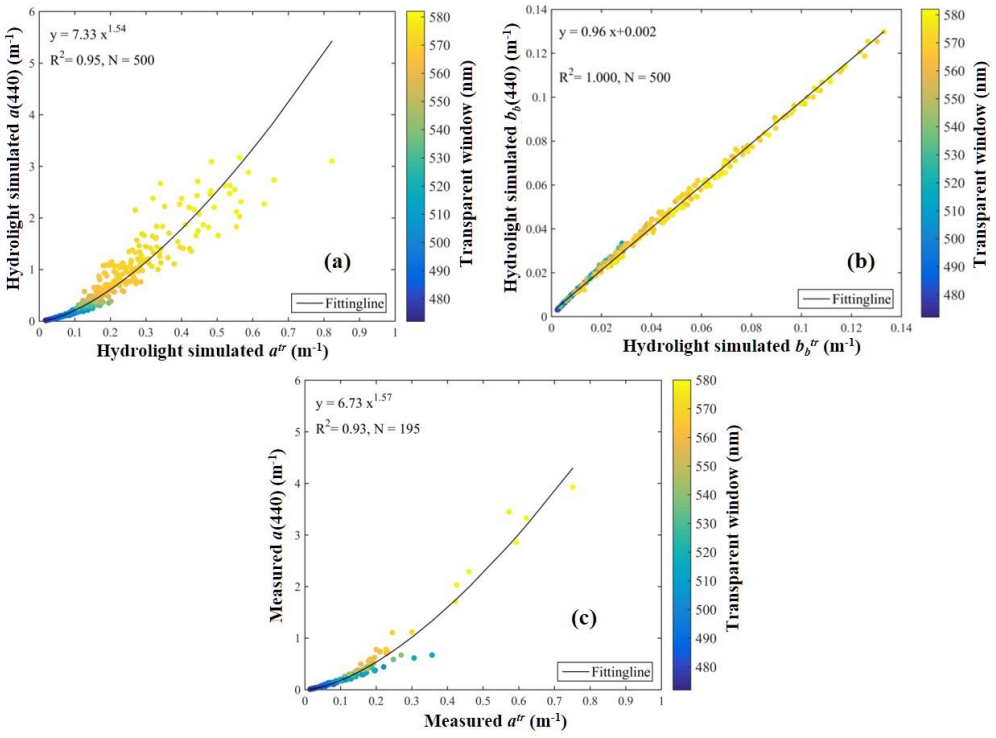

Fig. 9. Relationship between a^{tr}&b_b^{tr} and $a(440)$&$b_b(440)$. (a) a^{tr} versus $a(440)$ and (b) b_b^{tr} versus b_b (440) of the simulated data set; (c) a^{tr} versus $a(440)$ of the measurement data set.

The retrieved R_{rs}, a and b_b in the FZ2ab scheme are all related to a specific spectral region: water's transparent window. The dominant wavelength of this window, which varies with constituents in water [26,61], can be calculated from an R_{rs} spectrum though [26]. In addition, the *FUI* of water is closely associated with dominant wavelength [40]. All these features imply that the *FUI* is not only related to R_{rs} spectrum from which it was calculated, but also indicates the dominant wavelength of water's transparent window, thus provides a clear indication of the wavelength of the derived a^{tr} and R_{rs}^{tr} values. Actually, it is found that there are strong relationships between a^{tr} and b_b^{tr} and $a(440)$ and $b_b(440)$ (Fig. 9), respectively, so knowing a^{tr} and b_b^{tr} provides important properties for further evaluation of other water quality properties, such as Chla. This may further support the value of a^{tr}&b_b^{tr} for water quality products in both historical and modern marine study. It is noteworthy that the *FUI* in the data sets of this study was calculated using the in situ R_{rs} spectrum [27,15] rather than traditionally measured *FUI* along with a Secchi disk in water. Nevertheless, the accuracy of this calculated *FUI* was very high given the qualitative and classification nature of *FUI* measurement [27,15].

In summary, an inversion system FZ2ab was proposed to derive the IOPs of oceans from two historical water color measurements (*FUI* and Z_{SD}). R_{rs} was firstly estimated from *FUI* and Z_{SD} and then the total absorption (a) and backscattering (b_b) coefficients were algebraically solved as both R_{rs} and Z_{SD} are functions of a and b_b. Applications of this scheme to both HydroLight simulated and field measured data sets show very satisfactory and consistent results. Therefore, absorption and backscattering coefficients can be derived from measurements of *FUI* and Z_{SD}, which not only opens the door to obtain more accurate estimation of Chla concentration or suspended sediments than that from Z_{SD} or FUI alone, but also potentially support to extend the data records of IOPs of the oceans to the past century during which no measurements by modern instrumentations were available. We envision that

Optics EXPRESS

such data products would significantly enhance our understandings of the optical properties of the oceans and greatly help in the evaluation of oceanic systems in a changing climate.

Funding

Strategic Priority Research Program of the Chinese Academy of Sciences (Grant No. XDA19080304); National Natural Science Foundation of China (Grant No. 41471308, No. 41576169 and No. 41776184); and Youth Innovation Promotion Association of Chinese Academy of Sciences (Grant No. 2015128).

Acknowledgments

We thank the three anonymous reviewers for the constructive comments and suggestions.

References

1. D. Antoine, "Bridging ocean color observations of the 1980s and 2000s in search of long-term trends," J. Geophys. Res. **110**(C6), C06009 (2005).
2. M. J. Behrenfeld, R. T. O'Malley, D. A. Siegel, C. R. McClain, J. L. Sarmiento, G. C. Feldman, A. J. Milligan, P. G. Falkowski, R. M. Letelier, and E. S. Boss, "Climate-driven trends in contemporary ocean productivity," Nature **444**(7120), 752–755 (2006).
3. H. M. Dierssen, "Perspectives on empirical approaches for ocean color remote sensing of chlorophyll in a changing climate," Proc. Natl. Acad. Sci. U.S.A. **107**(40), 17073–17078 (2010).
4. A. Longhurst, S. Sathyendranath, T. Platt, and C. Caverhill, "An estimate of global primary production in the ocean from satellite radiometer data," J. Plankton Res. **17**(6), 1245–1271 (1995).
5. H. R. Gordon, O. B. Brown, R. H. Evans, J. W. Brown, R. C. Smith, K. S. Baker, and D. K. Clark, "A semianalytic radiance model of ocean color," J. Geophys. Res. Atmos. **93**(D9), 10909–10924 (1988).
6. A. Morel and B. Gentili, "Diffuse reflectance of oceanic waters. II Bidirectional aspects," Appl. Opt. **32**(33), 6864–6879 (1993).
7. S. A. Garver and D. A. Siegel, "Inherent optical property inversion of ocean color spectra and its biogeochemical interpretation: 1. Time series from the Sargasso Sea," J. Geophys. Res. Oceans **102**(C8), 18607–18625 (1997).
8. Z. Lee, K. L. Carder, and R. A. Arnone, "Deriving inherent optical properties from water color: a multiband quasi-analytical algorithm for optically deep waters," Appl. Opt. **41**(27), 5755–5772 (2002).
9. T. J. Smyth, G. F. Moore, T. Hirata, and J. Aiken, "Semianalytical model for the derivation of ocean color inherent optical properties: description, implementation, and performance assessment: erratum," Appl. Opt. **46**(3), 429–430 (2007).
10. P. J. Werdell, B. A. Franz, S. W. Bailey, G. C. Feldman, E. Boss, V. E. Brando, M. Dowell, T. Hirata, S. J. Lavender, Z. Lee, H. Loisel, S. Maritorena, F. Mélin, T. S. Moore, T. J. Smyth, D. Antoine, E. Devred, O. H. F. d'Andon, and A. Mangin, "Generalized ocean color inversion model for retrieving marine inherent optical properties," Appl. Opt. **52**(10), 2019–2037 (2013).
11. A. Bricaud, C. Roesler, and J. R. V. Zaneveld, "In situ methods for measuring the inherent optical properties of ocean waters," Limnol. Oceanogr. **40**(2), 393–410 (1995).
12. E. Boss and J. R. V. Zaneveld, "The effect of bottom substrate on inherent optical properties: Evidence of biogeochemical processes," Limnol. Oceanogr. **48**(1part2), 346–354 (2003).
13. R. Röttgers and R. Doerffer, "Measurements of optical absorption by chromophoric dissolved organic matter using a point-source integrating-cavity absorption meter," Limnol. Oceanogr. Methods **5**(5), 126–135 (2007).
14. M. A. Frederick, *An atlas of Secchi disc transparency measurements and Forel-Ule color codes for the oceans of the world*, Naval Postgraduate School Monterey CA, (1970).
15. S. P. Garaba, A. Friedrichs, D. Voß, and O. Zielinski, "Classifying Natural Waters with the Forel-Ule Colour Index System: Results, Applications, Correlations and Crowdsourcing," Int. J. Environ. Res. Public Health **12**(12), 16096–16109 (2015).
16. M. R. Wernand, "On the history of the Secchi disc," J. Eur. Opt. Soc. Rapid Publ. **5**, 10013 (2010).
17. J. Busch, R. Bardaji, L. Ceccaroni, A. Friedrichs, J. Piera, C. Simon, P. Thijsse, M. Wernand, H. van der Woerd, and O. Zielinski, "Citizen Bio-Optical Observations from Coast- and Ocean and Their Compatibility with Ocean Colour Satellite Measurements," Remote Sens. **8**(11), 879 (2016).
18. S. D. Seafarers, S. Lavender, G. Beaugrand, N. Outram, N. Barlow, D. Crotty, J. Evans, and R. Kirby, "Seafarer citizen scientist ocean transparency data as a resource for phytoplankton and climate research," PLoS One **12**(12), e0186092 (2017).
19. S. Q. Duntley and R. Preisendorfer, *The visibility of submerged objects*, Final Report to Office of Naval Research, (1952).
20. R. W. Preisendorfer, "Secchi disk science: Visual optics of natural waters1," Limnol. Oceanogr. **31**(5), 909–926 (1986).
21. E. Aas, J. Høkedal, and K. Sørensen, "Secchi depth in the Oslofjord–Skagerrak area: theory, experiments and relationships to other quantities," Ocean Sci. **10**(2), 177–199 (2014).

Optics EXPRESS

22. R. P. Bukata, J. H. Jerome, and J. E. Bruton, "Relationships Among Secchi Disk Depth, Beam Attenuation Coefficient, and Irradiance Attenuation Coefficient for Great Lakes Waters," J. Great Lakes Res. **14**(3), 347–355 (1988).
23. S. Kratzer, B. Håkansson, and C. Sahlin, "Assessing Secchi and photic zone depth in the Baltic Sea from satellite data," Ambio **32**(8), 577–585 (2003).
24. Z. Lee, S. Shang, C. Hu, K. Du, A. Weidemann, W. Hou, J. Lin, and G. Lin, "Secchi disk depth: A new theory and mechanistic model for underwater visibility," Remote Sens. Environ. **169**, 139–149 (2015).
25. Z. Lee, S. Shang, K. Du, B. Liu, G. Lin, J. Wei, and X. Li, "Enhance field water-color measurements with a Secchi disk and its implication for fusion of active and passive ocean-color remote sensing," Appl. Opt. **57**(13), 3463–3473 (2018).
26. S. Wang, J. Li, Q. Shen, B. Zhang, F. Zhang, and Z. Lu, "MODIS-Based Radiometric Color Extraction and Classification of Inland Water With the Forel-Ule Scale: A Case Study of Lake Taihu," IEEE J. Sel. Top. Appl. Earth Obs. Remote Sens. **8**(2), 907–918 (2015).
27. M. R. Wernand, H. J. van der Woerd, and W. W. Gieskes, "Trends in ocean colour and chlorophyll concentration from 1889 to 2000, worldwide," PLoS One **8**(6), e63766 (2013).
28. M. R. Wernand, A. Hommersom, and H. J. van der Woerd, "MERIS-based ocean colour classification with the discrete Forel–Ule scale," Ocean Sci. Discuss. **9**(4), 2817–2849 (2012).
29. J. Pitarch, "Biases in ocean color over a Secchi disk," Opt. Express **25**(24), A1124–A1131 (2017).
30. J. Li, S. Wang, Y. Wu, B. Zhang, X. Chen, F. Zhang, Q. Shen, D. Peng, and L. Tian, "MODIS observations of water color of the largest 10 lakes in China between 2000 and 2012," Int. J. Digit. Earth **9**(8), 788–805 (2016).
31. S. Wang, J. Li, B. Zhang, E. Spyrakos, A. N. Tyler, Q. Shen, F. Zhang, T. Kuster, M. Lehmann, Y. Wu, and D. Peng, "Trophic state assessment of global inland waters using a MODIS-derived Forel-Ule index," Remote Sens. Environ. **217**, 444–460 (2018).
32. H. J. Woerd and M. R. Wernand, "True colour classification of natural waters with medium-spectral resolution satellites: SeaWiFS, MODIS, MERIS and OLCI," Sensors (Basel) **15**(10), 25663–25680 (2015).
33. L. Ceccaroni, F. Velickovski, M. Blaas, M. R. Wernand, A. Blauw, and L. Subirats, "Artificial Intelligence and Earth Observation to Explore Water Quality in the Wadden Sea," Earth Observation Open Science and Innovation **15**, 311–320 (2018).
34. H. J. Woerd and M. R. Wernand, "Hue-angle product for low to medium spatial resolution optical satellite sensors," Remote Sens. **10**(2), 180 (2018).
35. Z. Lee, S. Shang, C. Hu, and G. Zibordi, "Spectral interdependence of remote-sensing reflectance and its implications on the design of ocean color satellite sensors," Appl. Opt. **53**(15), 3301–3310 (2014).
36. J. L. Mueller, A. Morel, R. Frouin, C. Davis, R. Arnone, K. Carder, Z. P. Lee, R. G. Steward, S. Hooker, C. D. Mobley, S. McLean, B. Holben, M. Miller, C. Pietras, K. Knobelspiesse, G. Fargion, J. N. Porter, K. J. Voss, *Ocean Optics Protocols For Satellite Ocean Color Sensor Validation, Revision 4. Volume III: Radiometric Measurements and Data Analysis Protocols* (NASA, 2003).
37. Z. Lee, Y. H. Ahn, C. Mobley, and R. Arnone, "Removal of surface-reflected light for the measurement of remote-sensing reflectance from an above-surface platform," Opt. Express **18**(25), 26313–26324 (2010).
38. C. D. Mobley, *Hydrolight 3.0 Users' Guide*. SRI International, Menlo Park, California, (1995).
39. IOCCG, *Remote Sensing of Inherent Optical Properties: Fundamentals, Tests of Algorithms, and Applications, (ed. Z-P. Lee)*. Dartmouth, NS, Canada, International Ocean-Colour Coordinating Group (IOCCG). (Reports of the International Ocean-Colour Coordinating Group, No. 5) (2006).
40. S. Shang, Z. Lee, and G. Wei, "Characterization of MODIS-derived euphotic zone depth: Results for the China Sea," Remote Sens. Environ. **115**(1), 180–186 (2011).
41. S. Tassan and G. M. Ferrari, "A sensitivity analysis of the 'Transmittance–Reflectance' method for measuring light absorption by aquatic particles," J. Plankton Res. **24**(8), 757–774 (2002).
42. Q. Dong, S. Shang, and Z. Lee, "An algorithm to retrieve absorption coefficient of chromophoric dissolved organic matter from ocean color," Remote Sens. Environ. **128**, 259–267 (2013).
43. J. L. Mueller, "Overview of measurement and data analysis protocols," Ocean Optics Protocols for Satellite Ocean Color Sensor Validation, Revision **2**, 87–97 (2000).
44. CIE, C. *Commission internationale de l'eclairage proceedings*, 1931, Cambridge University, Cambridge, (1932).
45. S. Novoa, M. Wernand, and H. van der Woerd, "The Forel-Ule scale revisited spectrally: preparation protocol, transmission measurements and chromaticity," J. Eur. Opt. Soc. Rapid Publ. **8**(2013), 13057 (2013).
46. H. R. Gordon, "Can the Lambert-Beer law be applied to the diffuse attenuation coefficient of ocean water?" Limnol. Oceanogr. **34**(8), 1389–1409 (1989).
47. Z.-P. Lee, "A model for the diffuse attenuation coefficient of downwelling irradiance," J. Geophys. Res. **110**(C2), C02016 (2005).
48. Z. Lee, C. Hu, S. Shang, K. Du, M. Lewis, R. Arnone, and R. Brewin, "Penetration of UV-visible solar radiation in the global oceans: Insights from ocean color remote sensing," J. Geophys. Res. Oceans **118**(9), 4241–4255 (2013).
49. Y. Fan, W. Li, C. K. Gatebe, C. Jamet, G. Zibordi, T. Schroeder, and K. Stamnes, "Atmospheric correction over coastal waters using multilayer neural networks," Remote Sens. Environ. **199**, 218–240 (2017).
50. C. Goyens, C. Jamet, and T. Schroeder, "Evaluation of four atmospheric correction algorithms for MODIS-Aqua images over contrasted coastal waters," Remote Sens. Environ. **131**, 63–75 (2013).

Optics EXPRESS

51. C. Hu, L. Feng, and Z. Lee, "Uncertainties of SeaWiFS and MODIS remote sensing reflectance: Implications from clear water measurements," Remote Sens. Environ. **133**, 168–182 (2013).
52. D. Müller, H. Krasemann, R. J. W. Brewin, C. Brockmann, P.-Y. Deschamps, R. Doerffer, N. Fomferra, B. A. Franz, M. G. Grant, S. B. Groom, F. Mélin, T. Platt, P. Regner, S. Sathyendranath, F. Steinmetz, and J. Swinton, "The Ocean Colour Climate Change Initiative: I. A methodology for assessing atmospheric correction processors based on in-situ measurements," Remote Sens. Environ. **162**, 242–256 (2015).
53. S. B. Hooker and S. Maritorena, "An Evaluation of Oceanographic Radiometers and Deployment Methodologies," J. Atmos. Ocean. Technol. **17**(6), 811–830 (2000).
54. G. Zibordi and K. J. Voss, Field Radiometry and Ocean Color Remote Sensing', in V. Barale, J. F. R. Gower, and L. Alberotanza, (eds.) *Oceanography from Space: Revisited*. Dordrecht: Springer Netherlands, 307–334 (2010).
55. E. Leymarie, D. Doxaran, and M. Babin, "Uncertainties associated to measurements of inherent optical properties in natural waters," Appl. Opt. **49**(28), 5415–5436 (2010).
56. D. E. Parker, P. D. Jones, C. K. Folland, and A. Bevan, "Interdecadal changes of surface temperature since the late nineteenth century," J. Geophys. Res. Atmos. **99**(D7), 14373–14399 (1994).
57. D. G. Boyce, M. Lewis, and B. Worm, "Integrating global chlorophyll data from 1890 to 2010," Limnol. Oceanogr. Methods **10**(11), 840–852 (2012).
58. M. Wernand and W. Gieskes, *Ocean optics from 1600 (Hudson) to 1930 (Raman), Shifting interpretation of natural water colouring*, Union des Océanographes de France, Paris, France (2011).
59. S. Shang, Z. Lee, L. Shi, G. Lin, G. Wei, and X. Li, "Changes in water clarity of the Bohai Sea: Observations from MODIS," Remote Sens. Environ. **186**, 22–31 (2016).
60. A. Morel and J. L. Mueller, "Normalized water-leaving radiance and remote sensing reflectance: Bidirectional reflectance and other factors," Ocean Optics Protocols for Satellite Ocean Color Sensor Validation **2**, 183–210 (2002).
61. M. Lehmann, U. Nguyen, M. Allan, and H. J. Woerd, "Colour classification of 1486 lakes across a wide range of optical water types," Remote Sens. **10**(8), 1273 (2018).